The Annexin A3−Membrane Interaction Is Modulated by an N-Terminal Tryptophan†

Andreas Hofmann,*,‡,§ Céline Raguénès-Nicol,|| Béatrice Favier-Perron,||,⊥,# Jose Mesonero,|| Robert Huber,‡ Françoise Russo-Marie,|| and Anita Lewit-Bentley⊥

Max Planck Institut für Biochemie, D-82152 Planegg-Martinsried, Germany, ICGM, U332 INSERM, 22 rue Méchain, F-75014 Paris, France, and LURE, Bât. 209D, Centre Universitaire Paris-Sud, F-91405 Orsay, France

Received October 11, 1999; Revised Manuscript Received April 24, 2000

ABSTRACT: The crystal structure of annexin A3 (human annexin III) solved recently revealed a well-ordered folding of its N-terminus with the side chain of tryptophan 5 interacting with residues at the extremity of the central pore. Since the pore of annexins has been suggested as the ion pathway involved in membrane permeabilization by these proteins, we investigated the effect of the N-terminal tryptophan on the channel activity of annexin A3 by a comparative study of the wild-type and the W5A mutant in structural and functional aspects. Calcium influx and patch−clamp recordings revealed that the mutant exhibited an enhanced membrane permeabilization activity as compared to the wild-type protein. Analysis of the phospholipid binding behavior of wild-type and mutant protein was carried out by cosedimentation with lipids and inhibition of PLA_2 activity. Both methods reveal a much stronger binding of the mutant to phospholipids. The structure is very similar for the wild-type and the mutant protein. The exchange of the tryptophan for an alanine results in a disordered N-terminal segment. Urea-induced denaturation of the wild-type and mutant monitored by intrinsic fluorescence indicates a separate unfolding of the N-terminal region which occurs at lower urea concentrations than unfolding of the protein core. We therefore conclude that the N-terminal domain of annexin A3, and especially tryptophan 5, is involved in the modulation of membrane binding and permeabilization by annexin A3.

Annexins are soluble proteins that bind to membranes in a calcium-dependent manner (*1*, *2*). All members of the annexin family possess a conserved core formed by four homologous repeats and an N-terminal part which is variable in length and sequence (*3*, *4*). The conserved core binds calcium and phospholipids, while the N-terminal sequence is considered to impart specific functions to different annexins. In several annexins, it contains phosphorylation sites and in some, such as annexins A1, A2, and A9 (annexin XI), the site of interaction with other proteins. Modifications of the N-terminus have in some cases been shown to influence the membrane-binding properties of the conserved core (*2*). Although the physiological role of the annexins is still unclear, they are most likely involved in membrane trafficking and fusion (*5*). They have in vitro anticoagulant effects, as well as an antiinflammatory activity through the inhibition of phospholipase A_2. Some annexins interact with cytoskeletal proteins (*6*). It has also been shown that members of the annexin family are expressed in a growth-dependent manner (*7*) and are targets for cellular kinases. These results suggest that annexins are involved in cell proliferation and differentiation.

Furthermore, some members of the annexin family have been shown to possess membrane permeabilizing activity. Annexin A7 (synexin) was reported to be a calcium channel with a conductance of about 10 pS (*8*). Annexin A5 allows divalent cations to cross membrane bilayers with a slight preference for calcium (conductance of about 30 pS) over barium and magnesium. An annexin A5-treated membrane is also permeable to monovalent cations such as lithium, cesium, sodium, and potassium (*9*). Annexin A1 forms an ion channel which conducts both magnesium and potassium ions. Permeabilizing activity has also been reported for annexin A6 (*10*). Recently, Arispe and co-workers (*11*) investigated the fusion of matrix vesicles with planar lipid bilayers and observed multiconductance ion channel activity. As matrix vesicles are highly enriched with annexin A5, they compared this channel activity to that of annexin A5-treated liposomes fused with planar lipid bilayers. They conclude from the similarity of electrophysiological data that the channel activity of the former is due to annexin A5.

Three structural hypotheses have been put forward to explain this activity in the case of annexins. Pollard and co-workers (*12*) proposed that the annexin molecule would completely integrate in the membrane through a structural

† This work was supported by the Fonds der Chemischen Industrie (A.H.), by a fellowship from the Institut de Formation Supérieure Biomédicale (B.F.-P.), by the Association Claude Bernard, Ligue contre le Cancer (C.R.-N.), and by European Union Grant ERBBIO4CT960083 (Biotechnology).

* Corresponding author.

‡ Max Planck Institut für Biochemie.

§ Present address: NCI−FCRDC, Macromolecular Crystallography Laboratory, Program in Structural Biology, Frederick, MD 21702. Tel.: +01-301-846-5033, Fax: +01-301-846-7101, email: hofmanna@ncifcrf.gov.

|| ICGM, U332 INSERM.

⊥ Centre Universitaire Paris-Sud.

Present address: l'Oreal KII, 8-12 Impasse Barbier, F-92117 Clichy, France.

10.1021/bi992359+ CCC: $19.00
Published on Web 06/09/2000

rearrangement that would lead to a "TIM-barrel" structure. This hypothesis is, however, incompatible with electron microscopy data, which show that the shape of annexin A5 attached to phospholipids is essentially the same as in the crystal and that it is peripherally bound by its convex face where the calcium sites are located (*13*). Perpendicular to this face lies a central pore, lined with charged residues suggested to be the ion pathway (*14*). Several mutagenesis experiments were carried out to confirm this hypothesis. The mutation of glutamic acid 95 of annexin A5, located in the central pore, was shown to have effects on the permeabilizing activity (*15*). It was suggested that the interfacial location of annexins between the cytosol and the membrane and the electrostatic potential of the protein could provoke a local electroporation phenomenon (*16*). A third, more recent hypothesis was proposed by Lüecke et al. (*17*). It is based on the three-dimensional structure of annexin B12 (annexin XII) which forms a hexamer in the crystal, composed of two stacked planar trimers. The authors proposed a new mode of insertion of the annexins in a phospholipid bilayer. The double trimer of annexins might be fully integrated into the membrane in a calcium-dependent manner by locally rearranging phospholipid molecules. The hexamer possesses a central hydrophilic pore of about 8 Å diameter that was suggested as a putative ion pathway. This model has not been confirmed by experiment so far. Nevertheless, based on very recent experiments with annexin B12 at low pH, where membrane permeabilization activity was also found for this annexin (*18*), penetration of the phospholipid bilayer was proposed again, this time by an annexin monomer only, however. For this kind of insertion, the protein is supposed to undergo a complete structural rearrangement (*19*).

The three-dimensional structure of annexin A3 has recently been solved (*20*). The conserved core is similar to the annexin A5 structure, with four domains composed of five α-helices each. The N-terminal part of the protein, three amino acids longer compared to annexin A5, has a well-defined structure. Indeed, the first amino acids of annexin A3 are located at the cytosolic extremity of the central pore of the protein, with the side chain of tryptophan 5 inserting into it and forming hydrogen bonds and hydrophobic contacts with residues within the pore.

If this pore is the ion pathway, a difference in channel activity should be expected between wild-type annexin A3 and its W5A mutant. We therefore studied the permeabilizing activity of both proteins by calcium-influx measurements and by electrophysiological methods using patch−clamp experiments. The stability and membrane binding of both proteins were investigated to try to understand the mechanism of membrane permeabilization. We also analyzed the three-dimensional structure of the mutant W5A for comparison with the wild-type annexin A3.

Here we report that although neither protein exhibited a true channel activity, the mutant showed an enhanced membrane permeabilization activity correlated to a stronger binding to phospholipids. Even though the structure is very similar for the wild-type and the mutant protein, the exchange of the tryptophan for an alanine results in a disordered N-terminal segment. We propose that the N-terminal domain of annexin A3, and within it tryptophan 5, is involved in the modulation of membrane binding and permeabilization by annexin A3.

MATERIALS AND METHODS

Preparation of Proteins. Annexin A3 cDNA was obtained from a pUC plasmid (BIOGEN, Cambridge, MA) using the *Eco*RI restriction enzyme. After digestion with *Sec*I, oligonucleotides were linked to complete the cDNA sequence encoding annexin A3 and to create a *Bam*HI cloning site. The cDNA sequence was then cut by *Bam*HI and *Eco*RI restriction enzymes and introduced into a pGEX-2T vector (Pharmacia, France) to produce a GST fusion protein.

The W5A mutant of annexin A3 was prepared by site-directed mutagenesis. The *Bam*HI/*Eco*RI fragment of the vector pGEX-2T containing the complete annexin A3 cDNA was cloned into the corresponding site of the Bluescript II KS+ vector. The desired mutation was introduced by oligonucleotide-directed mutagenesis using the procedure of Kunkel (*21*). The mutant W5A was produced with the synthetic oligonucleotide 5′-pGGA TCC GCA TCT ATC GCG GTT GGA CAC CGAp-3′. The mutated annexin A3 cDNA insert was purified by agarose gel electrophoresis and cloned again into the pGEX-2T vector. The cDNA of the mutant was sequenced in its full length to verify the presence of the desired mutation. Both proteins were isolated and purified (including removal of the GST moiety) using the protocol for the wild-type protein (*20*).

Phospholipase A_2 Activity Measurement (PLA_2 Assay). PLA_2[1] activity was measured as described in ref *22*. Vesicles of 1-hexadecanoyl-2-(1-pyrenedecanoyl)-*sn*-glycero-3-phosphoglycerol ammonium salt (*β*-py-C10-PG, Molecular Probes, The Netherlands) were prepared at 2 mM in 1 mL of buffer containing 50 mM TRIS-HCl (pH 7.5), 0.5 M NaCl, and 1 mM EGTA. The reaction was carried out by adding sequentially 0.1% fatty acid free BSA (Sigma), 10 μL of the protein to be tested, and 1 μg of bee venom PLA_2 (Sigma), yielding a final concentration of 70 nM enzyme, and 10 mM $CaCl_2$. The proteins tested were annexin A3 wild-type and mutant W5A at final concentrations of 3, 15, 30, and 150 nM, 3 μM, and 15 μM. The activity was recorded as the monomer emission of pyrene, using a spectrofluorometer (Jobin-Yvon, France). Fluorescence emission was measured for each condition in six independent experiments. To test whether the values obtained for each group are significantly different, while allowing for experimental error, the probability of differences between experimental groups, *p*, was determined by a two-tailed Student's *t*-test. $p < 0.05$ indicates a significant difference between two groups.

Phospholipid Binding Measurement. Ca^{2+}-dependent phospholipid binding properties of annexin A3 were measured using a liposome-pelleting assay (*23*). Phosphatidylserine and phosphatidylcholine (Avanti Polar Lipids, reference numbers 830034 and 850375, respectively) in chloroform were mixed in a 1:4 ratio, dried under nitrogen, then resuspended in 10 mM PIPES, pH 6.8, at 2 mg/mL, and sonicated to form liposomes. Calcium buffers with a free Ca^{2+} concentration of 10^{-8} or 10^{-3} M were prepared using the software CHELATE (*24*) with dissociation constants from (*25*). Annexin binding to liposomes was carried out by incubating

[1] Abbreviations: PE, phosphatidylethanolamine; PIPES, 1,4-piperazinediethanesulfonic acid; PLA_2, phospholipase A_2; PS, phosphatidylserine; TRIS, tris(hydroxymethyl)aminomethane. Annexin nomenclature in the present work follows the recommendations by Morgan et al. (*48*).

100 μg of protein with 100 μL of liposomes in a final volume of 200 μL of PIPES (10 mM, pH 6.8) for 20 min at different calcium concentrations. After a 47000*g* centrifugation for 15 min, the supernatant was washed in 200 μL of calcium buffer. After a second centrifugation step, the pellet was resuspended in 50 μL of PIPES (10 mM, pH 6.8) containing 5 mM EDTA and 1% Triton X-100. Then 20 μL of the first supernatant and of the pellet was loaded on 12% SDS−PAGE and then silver stained. Densitometric analysis with ImageQuant 1.2 was performed to quantify annexin bound to the PS/PC liposomes. Data points in figures represent a mean of 3−5 experiments. As mentioned above, the probability of differences between various conditions was determined by a two-tailed Student's *t*-test, and $p < 0.05$ indicates a significant difference between two groups.

Estimation of Lipid-to-Protein Ratio. A geometric estimation of lipid and protein surface was done. Taking the numbers from Reeves and Dowben (*26*), one obtains for a lipid concentration of $c(\text{lipid}) = 84$ μM a vesicle concentration of ${}^1N(\text{ves}) = 5.9 \times 10^8$ mL^{-1}. The lipid amount per vesicle, $\nu(\text{lipid})$, can be calculated according to

$$\nu(\text{lipid}) = \frac{N(\text{lipid})}{N(\text{ves})} = \frac{c(\text{lipid})^* N_A}{{}^1N(\text{ves})} \quad (1)$$

with N being the actual number, N_A Avogadro's constant, and ${}^1N$ the vesicle concentration.

The total accessible lipid surface, A, is dependent on the amount of lipid present in the sample:

$$A = a^* N(\text{ves}) = \frac{a^* n(\text{lipid})^* N_A}{\nu(\text{lipid})} \quad (2)$$

where a is the specific (molar) surface and n the molar amount; N, ν, and N_A are as above.

For $n(\text{lipid}) = 0.4$ μmol (assuming 200 μg of lipids with an average molecular mass of $M = 530$ g/mol), this expression yields a surface of $A(\text{lipid}) = 33 \times 10^{-3}$ m^2 with $a(\text{lipid}) = 11.7$ μm^2. On the other hand, assuming a specific surface of $a(\text{anx}) = 28.9 \times 10^6$ m^2/mol, an amount of $n(\text{anx}) = 2.8$ nmol (corresponding to a concentration of $c(\text{anx}) = 14$ μM) results in a total protein surface of $A(\text{anx}) = 81 \times 10^{-3}$ m^2.

If we assume a monolayer of protein on the liposome surface, this means a 2.5-fold excess of annexin with respect to the total accessible lipid surface. The lipidic component in the phospholipid binding assays is thus expected to be limiting.

Urea-Induced Unfolding. Determination of the folding stability of wild-type and mutant protein was carried out by recording fluorescence spectra of the proteins in the absence and in the presence of varying concentrations of urea. The samples consisted of 10 mM TRIS-HCl (pH 7.5) and the desired amount of urea added from a 10 M stock solution. Both proteins were added from a stock solution (final concentration: 40 μg/mL) 15 min prior to fluorescence measurements. The total sample volume was in each case 300 μL. Fluorescence emission spectra were recorded on a Perkin-Elmer LS 50B luminescence spectrometer using two excitation wavelengths, at $\lambda_{exc} = 280$ nm and $\lambda_{exc} = 295$ nm, respectively. All fluorescence spectra were corrected against buffer-only samples and analyzed off-line with the PeakFit software (Jandel Scientific). All experiments were carried out independently 3 times.

Annexin-Induced Calcium-Influx Assay (FURA-2 Assay). The calcium influx into liposomes was monitored using the calcium-sensitive dye FURA-2 (*27*), using the FURA-assay protocol described in ref *28*. Phospholipid vesicles were prepared according to Reeves and Dowben (*26*) by mixing phosphatidylserine and phosphatidylethanolamine (Avanti Polar Lipids) in a molar ratio of 3:1 in choloroform (total lipid amount approximately 1 μmol). The solution was dried under a stream of nitrogen for 30 min and then exposed to a stream of water-saturated nitrogen for another 30 min. The lipid film was covered with 2 mL of buffer F1 (100 μM FURA-2, 180 μM EDTA, 162 mM saccharose, 5 mM HEPES, pH 7.4) and incubated for 2 h at 37 °C. The vesicles were separated by centrifugation at 12000*g* for 30 min. After resuspension in 200 μL of buffer F2 (200 μM EDTA, 180 mM sucrose, 10 mM HEPES, pH 7.4), they were centrifuged again, resuspended in buffer F2, and applied to an S200 spin column (Pharmacia). After two additional centrifugation steps, the liposome pellet was finally resuspended in 200 μL of F2. The final collection step was done by centrifugation at 12000*g* for 30 min.

To increase the stability of the FURA−liposomes, all solutions were saturated with argon. A 20 μL aliquot of the FURA-loaded liposome suspension was mixed with 475 μL of buffer F2, and 5 μL of a 50 mM $CaCl_2$ solution was added, bringing the final concentration of calcium to 500 μM. The fluorescence intensity was measured at 510 nm with the sample excited at 340 and 380 nm in time intervals of 1 min. After an equilibration time of 4 min, the protein was added from a concentrated stock solution (final concentration: 1 μM). Fluorescence measurements were performed on a Perkin-Elmer 650-40 fluorescence spectrophotometer with a spectral bandwidth of 5 nm for the excitation and emission slits, respectively. The shutter was closed between the measurements to avoid photobleaching effects. Intensity measurements were carried out at 1 min intervals. At $t = 36$ min, 3 μL of a solution of Br-A23187 (0.1 mg/mL) was added to achieve the maximal possible calcium signal. Fluorescence monitoring was continued until $t = 40$ min. Each experiment was carried out independently 3 times.

Data analysis was performed by normalizing the fluorescence ratio $F(340\text{ nm})/F(380\text{ nm})$ with respect to the maximal possible fluorescence ratio obtained from the values from 36−40 min. The normalized fluorescence ratio f was plotted vs time, thereby yielding an influx curve. These curves were further analyzed by calculating the slope α of the time interval 15−35 min as an activity parameter ("steady state"), and the initial slope β at $t = 4$−5 min.

Electrophysiological Measurements. Membrane permeabilization activity of annexin A3 wild-type and the mutant W5A was investigated using single channel recordings (*29*). Seals were formed from PS/PE (molar ratio 4:1) on patch pipets (quartz, outer diameter 1.0 mm) with an opening diameter of about 1 μm using the double-dip method (*30*). Then 3.5 μL of lipid mixture in a pentane/chloroform/ethanol solution (0.25 μg/mL) was spread onto the surface of a 150 μL drop of the sealing solution (50 mM $MgCl_2$, 20 μM $CaCl_2$, 10 mM HEPES, pH 7.4). The seals had resistances of 5−10 GΩ. The pipet solution contained 50 mM $MgCl_2$, 10 mM HEPES, pH 7.4, in every experiment. Magnesium

Table 1: Diffraction Data Statistics

parameter	
resolution (Å)	1.8
total no. of observations	70749
no. of unique reflections	25932
R_{sym}[a]	0.049
completeness of data	96.1%
completeness in last bin	95.2%
$I > 2\sigma(I)$	97.0%
$I > 2\sigma(I)$ in the last bin	63.2%

[a] $R_{sym} = \Sigma(I_i - \langle I \rangle)/\Sigma I_i$ for equivalent reflections, where I_i is the intensity of an individual measurement and $\langle I \rangle$ is the mean value.

Table 2: Refinement Statistics[a]

parameter	
total no. of non-hydrogen atoms	2510
no. of solvent molecules	227
no. of calcium ions	6
amplitude cutoff	1 $\sigma(F)$
no. of reflections used	25287
R-factor	0.198
R_{free}	0.207
mean *B*-factor (Å^2)	19.5
rms deviations from standard values	
bonds (Å)	0.005
planes (Å)	0.013
angles (deg)	2.359
chiral volumes (Å^3)	0.072
B-factor on main chain bonds (Å^2)	3.57
Ramachandran plot	
residues in most favored regions	96.2%
residues in further allowed regions	3.8%

[a] rms, root-mean-square. *R*-factor $= \Sigma||F_o| - |F_c||/\Sigma|F_o|$, where F_o and F_c are the observed and calculated structure factors, respectively. R_{free} defined in (*46*).

was chosen because of its indifferent effect on the binding behavior of annexins (*31*) and the stabilizing properties of this cation on acidic phospholipid bilayer membranes. After testing the seal over the whole voltage range and correcting the offset potential, protein was added to a final concentration of 2 fM. If binding was observed (resistance increased), the bath solution was exchanged for the appropriate cation solution, i.e., either 100 mM chloride salt of a monovalent cation or 50 mM chloride salt of a divalent cation, in 10 mM HEPES, pH 7.4.

Currents were recorded using an EPC-7 amplifier (List Medical, Darmstadt, Germany) and sampled at 10 kHz after filtering at 3 kHz with a sample duration of 12.7 s. All recordings were made at 19 °C. Data analysis was performed after refiltering at 500 Hz with the pClamp software package (V5, Axon Instruments) and the Strathclyde Electrophysiology Software (WCP V1.2/PAT v 7.0, J. Dempster, Glasgow, Scotland), respectively, and all-points-amplitude histograms were generated.

Crystal Structure of the Annexin A3 W5A Mutant. Parallelepipedic crystals were obtained by vapor diffusion using ammonium sulfate as a precipitant. The drop of 2 μL contained 15.5 mg/mL protein, 20 mM $CaCl_2$, and 20% $(NH_4)_2SO_4$ in 50 mM TRIS-HCl buffer at pH 7.5. The well contained 50% $(NH_4)_2SO_4$ in the same buffer. The crystals were monoclinic, space group $P2_1$, with cell dimensions $a = 42.82$ Å, $b = 68.86$ Å, $c = 50.87$ Å, $\beta = 96.12°$, and one molecule per asymmetric unit.

Data were measured on the DW32 station on the DCI synchrotron ring at LURE, Orsay, which is equipped with a MARresearch imaging plate detector (*32*), using a wavelength of 0.99 Å and a crystal-to-detector distance of 120 mm. The data reduction was performed using the MarXDS program (*33*) and the CCP4 program suite (*34*). The data quality is summarized in Table 1. Crystals were isomorphous to those of wild-type annexin A3 (*20*).

Starting from the annexin A3 wild-type structure, refinement was initiated with XPLOR (*35*), using conjugate gradient minimization. A $3F_o - 2F_c$ map was calculated and used for a manual reconstruction on a graphics terminal with FRODO (*36*). Further rounds of refinement consisting of simulated annealing were finally completed with PROLSQ (*37*) to obtain good geometry. Table 2 summarizes the refinement results.

RESULTS

The Crystal Structure of Annexin A3-W5A. The structure of the annexin A3-W5A mutant is nearly identical to that of the wild-type protein. The only difference concerns the N-terminal part, where in the new structure residues 3−9 are not defined in the electron density map, therefore indicating considerable flexibility of that region. The wild-type structure, on the other hand, reveals hydrogen bonding of Trp-5 with Glu-127 and hydrophobic interactions of the aromatic residue with Ile-282 (*20*). Nevertheless, the absence of interactions at the level of residue 5 does not affect the conformation of the hydrophilic pore formed by helices IIA, IIB, IVA, and IVB (Figure 1). A detailed comparison of the wild-type and the mutant structure shows differences in the Cα positions of 0.2−0.3 Å in the region close to Trp-5: the extended chain connecting domains II and III, and in the loops between helices B and C of all four domains. Surprisingly, the calcium loops in all domains are also displaced by 0.3−0.4 Å. Both structures display comparable *B*-factors. The first two visible residues in the mutant structure have naturally a higher *B*-factor than the equivalent residues in the wild-type strucure.

The calcium-binding loop in domain II is somewhat more disordered in the mutant compared to the wild-type structure. Domain III has several calcium sites: one principle site in the calcium-binding loop itself and two secondary sites with only two to three protein ligands. We had observed the binding of a small molecule, that we interpreted as ethanolamine, to one of these secondary calcium ions (*38*). In this domain, we observe the same number of calcium ions bound to the wild-type and to the W5A mutant of annexin A3, as well as the molecule of ethanolamine. In the mutant structure, however, the ethanolamine is better defined and the calcium interacting with it has full occupancy, while it had been refined with only 0.5 occupancy in the wild-type structure.

Inhibition of PLA_2 Activity. The inhibition of PLA_2 activity by annexin is most likely due to competition for phospholipid binding. Both the annexin A3 wild-type and the W5A mutant decrease PLA_2 activity in a dose-dependent manner (Figure 2). Surprisingly, the extent of PLA_2 inhibition is significantly enhanced with the W5A mutant when compared to the wild-type protein. The dose−response curves (Figure 2A) show that at low concentrations (0.1−5 μg/mL) annexin A3-W5A is a stronger inhibitor of PLA_2 activity than annexin A3 wild-

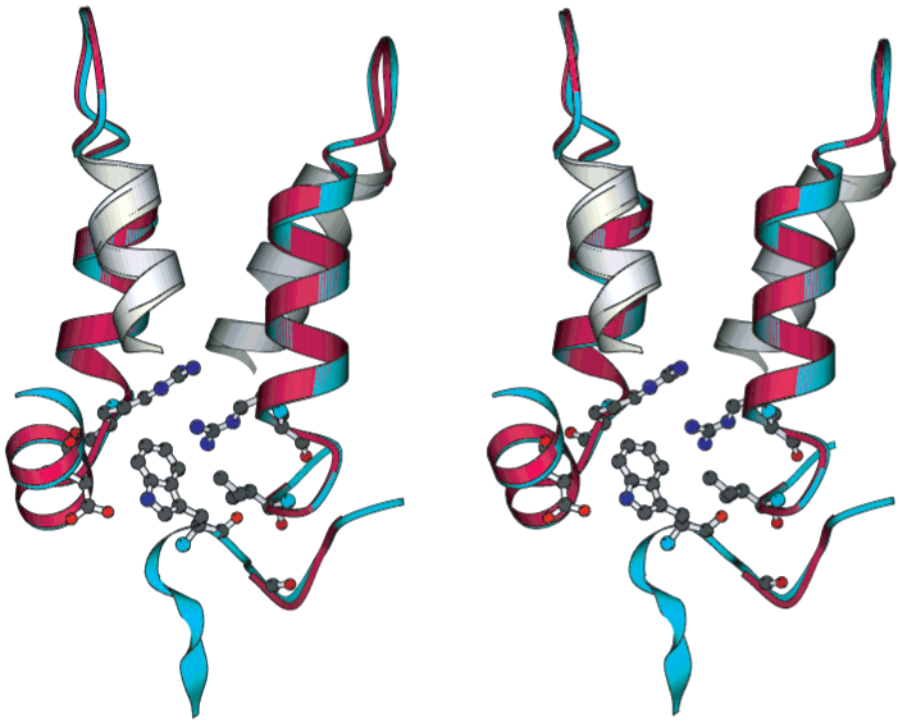

FIGURE 1: Superposition of the N-terminal region and the helices lining the central pore (helices A, B, and C of domain II, helices A and B of domain IV) of annexin A3 wild-type (blue) and its W5A mutant (red). Amino acid side chains mentioned in the text (Arg-120, Glu-127, Arg-127, Ile-282) are highlighted, as well as Trp-5 (wild-type) and the first visible amino acid in the mutant structure (Ala-9). Figure prepared with MOLSCRIPT (*47*).

type. The initial slopes are significantly different, having values of $\alpha_1 = -6.1\%$ (mL/μg) for the wild-type and $\alpha_2 = -14.9\%$ (mL/μg) for the mutant protein. At steady-state (50 μg/mL), annexin A3 and its mutant inhibit about 50% of PLA_2 activity, and the difference between the two proteins is no longer significant (Figure 2B).

Binding of Annexin A3 to PS/PC Liposomes. For both wild-type and mutant annexin A3, the binding to PS/PC liposomes is dependent on free calcium concentration in the range tested (0.01 μM to 1 mM). In the presence of low concentrations of calcium (i.e., at 0.01 μM Ca^{2+}), we observed some binding for the two proteins: 4−6% of the total protein is found co-pelleted with lipids. In the presence of 10 μM calcium, differences persist between the W5A mutant and the wild-type protein that become significant at 100 μM calcium (14% for W5A, versus 8% for the wild-type proteins, bind to liposomes). At 1 mM calcium concentration, binding to lipids increases sharply: 45% of W5A and 40% of wild-type protein associate with liposomes (Figure 3). This behavior merits attention since testing of a variety of other single mutants with the site of mutation at potentially important amino acids shows no statistically significant difference in phospholipid binding when compared to the wild-type protein (data not shown). It is noteworthy that even in the absence of calcium there is binding to the liposomes which is significantly different for both proteins: 6.3% of the W5A mutant and 3.8% of the wild-type are bound to the vesicles, respectively. As mentioned under Materials and Methods, the estimation of lipid-to-annexin ratio reveals that the amount of lipids present in the assay is the limiting component accounting for the observed saturation at ca. 45%.

Urea-Induced Unfolding. In the W5A mutant there is only one tryptophan residue (Trp-190) which contributes to the spectrum, while there are two tryptophans in wild-type annexin A3, Trp-5 and Trp-190. A comparison of the fluorescence behavior of the two proteins in the native state can help to distinguish the contribution of the two tryptophans. The unfolding curves for annexin A3 wild-type and the W5A mutant differ in both the change of intensity at the maximum emission wavelength, as well as the change of the wavelength at maximum emission (Figure 4). At $\lambda_{exc} =$ 295 nm, only tryptophan residues are selectively excited, while at $\lambda_{exc} = 280$ nm there is a contribution from tryptophan and tyrosine residues. When comparing the two excitation wavelengths, we see an increase in the maximum of the fluorescence emission of the mutant from 328 to 348 nm when the excitation wavelength is tuned to either 280 or 295 nm, respectively. The tyrosine emission is therefore far from negligible at 280 nm. On the contrary, the maximum of the fluorescence emission of the wild-type protein is the same at both excitation wavelengths and is characteristic of tryptophan emission (341 nm at $\lambda_{exc} = 280$ nm and 342 nm at $\lambda_{exc} = 295$ nm). This means that the fluorescence emission of the wild-type annexin A3 is dominated by Trp-5 whatever the excitation wavelength.

The different behavior seen for the wild-type and the mutant proteins in urea denaturation experiments is due to different regions of the protein being observed in the two cases. When selectively exciting the unique Trp-190 residue in the W5A mutant, we see an increase to 133% (Figure 4A), while the emission maximum undergoes a red-shift of about 10 nm upon urea-induced unfolding (Figure 4B). When using an excitation wavelength of 280 nm, when both tryptophan and tyrosine residues contribute to the fluorescence, we observe an increase in the emission intensity to 120% (Figure 4C) and a large red-shift of 26 nm with increasing urea concentration (Figure 4D).

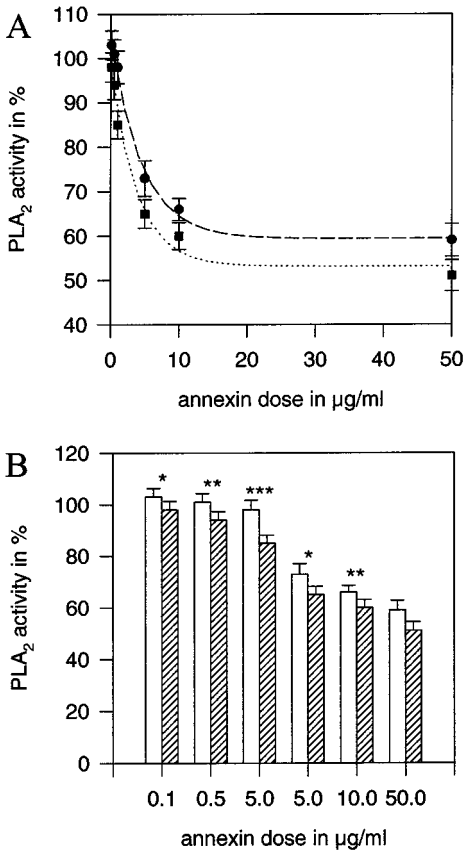

FIGURE 2: Inhibition of PLA_2 activity by annexin A3 wild-type and mutant W5A. (A) Dose−response curves of annexin inhibition of PLA_2 activity. Wild-type annexin A3 is represented as circles and the W5A mutant as squares. Initial slopes of the curves are $\alpha_1 = -6.1\%$ (mL/μg) and $\alpha_2 = -14.9\%$ (mL/μg) for wild-type and mutant, respectively. (B) Histograms representing the numeric values of the curves (white boxes, wild-type; hatched boxes, W5A mutant). Significance of differences between the two proteins is indicated by asterisks: (*) $p < 0.05$, (**) $p < 0.01$, (***) $p < 0.005$. The data depicted represent a mean of six independent measurements.

The situation is strikingly different for the wild-type protein. The emission intensity decreases upon unfolding of the protein for both excitation wavelengths (Figure 4E,G), while the red-shift of the emission maximum for tryptophan is larger (13 nm, $\lambda_{exc} = 295$ nm; Figure 4F) than for both tryptophan and tyrosine (11 nm, $\lambda_{exc} = 280$ nm; Figure 4H). The intensity and wavelength curves for $\lambda_{exc} = 295$ nm show a two-step behavior: one transition at about 0.7 M urea and a second one at about 3.5−4 M urea. If we assume that the two tryptophan residues in the wild-type protein will have the same environment when the protein is completely unfolded, we can compare the relative intensity change at $\lambda_{exc} = 295$ nm for the two proteins. The latter part of the intensity curve for the wild-type protein resembles that of the mutant, with a similar transition region. We can therefore conclude that the first step of the unfolding curve for the wild-type protein corresponds to the release of the N-terminal domain (Trp-5), followed by the unfolding of the rest of the protein (Trp-190).

Calcium-Influx Assay. The W5A mutant shows differences in the calcium-influx assay with FURA-2-loaded liposomes (Figure 5) when compared to the wild-type annexin A3. The calcium-influx curves are shown in Figure 5A−C. They show a higher influx activity for the W5A mutant, though with

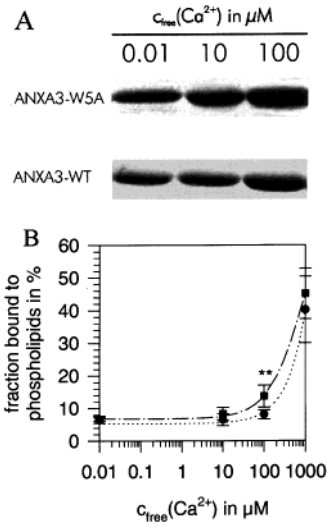

FIGURE 3: Phospholipid binding of wild-type and W5A annexin A3 at different calcium concentrations quantified after silver-stained SDS−PAGE of proteins bound to liposomes. (A) Silver-stained SDS−PAGE of liposome-bound annexin A3 wild-type or W5A with different free calcium concentrations. (B) Quantification of the plots showing the significance of differences between the two proteins. The wild-type annexin A3 is represented as circles and the W5A mutant as squares. All data are presented as mean ± standard deviation of 3−5 experiments [significance: (**) $p < 0.01$].

only moderate accuracy. For the purpose of comparison, the influx curves were analyzed with respect to the two slopes, α and β, as described under Materials and Methods (Figure 5D). The steady-state slope α reveals a 3-fold higher calcium influx rate, while the initial slope β shows an approximately 5-fold higher calcium influx rate for the W5A mutant compared to the wild-type protein.

Investigation of Membrane Permeabilization by Electrophysiological Methods. When tested in patch−clamp experiments, only the mutant W5A displays membrane permeabilizing activity due to a cation flux through the membrane. No changes in membrane permeabilizing activity are observed with different anions (chloride, sulfate; data not shown). A simple system with symmetrical ionic conditions was chosen: bath and pipet each contained 50 mM $MgCl_2$ with an extra 20 μM $CaCl_2$ present in the bath to allow the binding of annexin to the membrane. After clamping a negative potential over the membrane, the appearance of different opening levels rather than a single predominant level is frequently observed, as illustrated by Figure 6A. Although the current recordings look very similar to those from intrinsic ion channels, the activity displayed by annexin-treated patches does not occur with a regular amplitude as one would expect for an ion channel. Furthermore, while the wild-type protein does not display any activity (Figure 6B), the mutant shows an increased activity in permeabilizing the membrane under symmetrical $MgCl_2$ conditions (Figure 6A). We also studied sodium and potassium as the conducting cation in the bath and found Ohmic current−voltage relations with nearly no shift in the reversal potential for all cations tested (data not shown). Data analyses carried out by all-points-amplitude histograms, generated for each current recording, confirm the difference between the wild-type protein (6D) and the mutant (6C) as far as provoking a different membrane permeabilization activity. This differential behavior was observed for all batches of wild-type

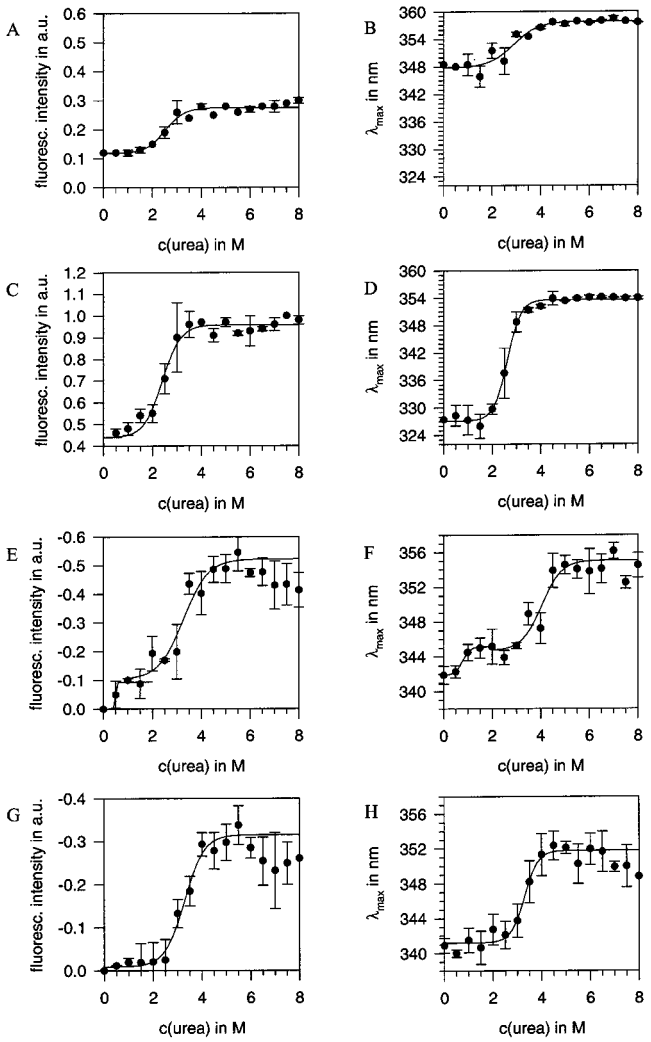

FIGURE 4: Urea-induced unfolding as monitored by intrinsic fluorescence. Unfolding curves are plotted as the intensity at the emission maximum and as the maximum emission wavelength as a function of urea concentration. The data shown represent the average of three independent experiments. Annexin A3-W5A with $\lambda_{exc} = 295$ nm (A, B) and $\lambda_{exc} = 280$ nm (C, D). Annexin A3 wild-type with $\lambda_{exc} = 295$ nm (E, F) and $\lambda_{exc} = 280$ nm (G, H).

and mutant proteins tested in a large number of experiments (10−15 independent setups for an individual ion condition and protein).

Taken together, our data do not allow us to conclude reliably that the annexin A3-W5A mutant behaves as a conventional channel, but rather that it induces an increased nonspecific cationic pemeabilization activity.

DISCUSSION

When the N-terminal Trp residue of annexin A3 is mutated (W5A mutant), the interaction of the protein with membranes is modified significantly. The membrane permeabilization activity of the mutant is enhanced as revealed by the influx rates obtained from the calcium-influx assay and the electrophysiological recordings. The inhibitory effect on PLA_2 activity is also significantly enhanced for the mutant. Since the inhibition of PLA_2 is most likely a consequence of competition for phospholipid binding, this parameter was investigated using a liposome-binding assay. Both results indicate that the membrane-binding capacity of annexin A3 is enhanced when the N-terminal tryptophan is exchanged for alanine. The crystal structures of both proteins are very similar, with only small differences in atomic positions and thermal parameters. The calcium ions seem better defined in the mutant structure, which could be due to a higher concentration of calcium used in the crystal preparation (20 mM vs 10 mM for the wild-type protein, both with ammonium sulfate as a precipitant). The most interesting difference is in the way the ethanolamine molecule is bound. Its density, and even more that of the adjacent calcium ion, is much better defined in the mutant structure. One can argue that this molecule is mimicking one of the possible phospholipid headgroups, which it resembles (*38*). This structural detail might therefore be suggesting that the removal of the N-terminal tryptophan, which blocks the central pore of annexin A3, could facilitate interactions of the protein at its opposite surface.

Urea unfolding studies in the present work further support the hypothesis of allosteric regulation of the membrane activity of annexin A3. The unfolding displays a two-step process; in the first step, the N-terminal tryptophan residue is released, after which the unfolding proceeds in a similar manner for both the wild-type and the mutant protein. This result emphasizes the important role of this residue for the overall conformational flexibility of annexin A3.

The results from the FURA-assay describe the macroscopic behavior of annexins interacting with membrane bilayers, since the effective membrane surface is much larger in the calcium-influx assay compared with electrophysiological experiments. The influx assay might therefore serve as a general tool for comparative studies of the membrane permeabilization activity of annexins, as shown recently for annexins A1, A2, A5, and A6 (*39*). While the wild-type A3 protein displays only small calcium-influx rates in the FURA-assay, the rates obtained with its W5A mutant are significantly higher. This difference is clearly due to the loss of the N-terminal tryptophan side chain. If the central pore of the protein is the ion pathway, the enlarged activity of the mutant could be explained by the occluding effect of the Trp-5 residue at the pore entrance, this side chain being involved in hydrogen bonds with Glu-127 and in hydrophobic interactions with Ile-282 (Figure 1). The absence of these constraints might influence the conformation or ensemble of conformations of the protein core both in solution and in the membrane-bound state, as well as their interconversions. The mutant might have altered flexibility which can affect its binding behavior, and this in turn affects membrane permeabilization. In their recent study, Arbolades and coworkers (*40*) correlate the presence/absence of an N-terminal part of annexin A5 with several parameters influencing protein stability and membrane interaction. Similar results were obtained with annexin A5 truncation mutants where the N-terminal part is successively truncated (*41*). Taken together, our data on annexin A3 and its W5A mutant using the calcium-influx experiments, rather than arguing for annexin A3 W5A mutant acting as a specific ion channel, favor another hypothesis: calcium influx may stimulate the formation of new annexin-induced nonspecific cationic channels, which in turn stimulate further calcium influx, a process that takes place on a time scale of minutes. The difference in the calcium influx may be a consequence of the difference in the flexibility of the protein, and therefore

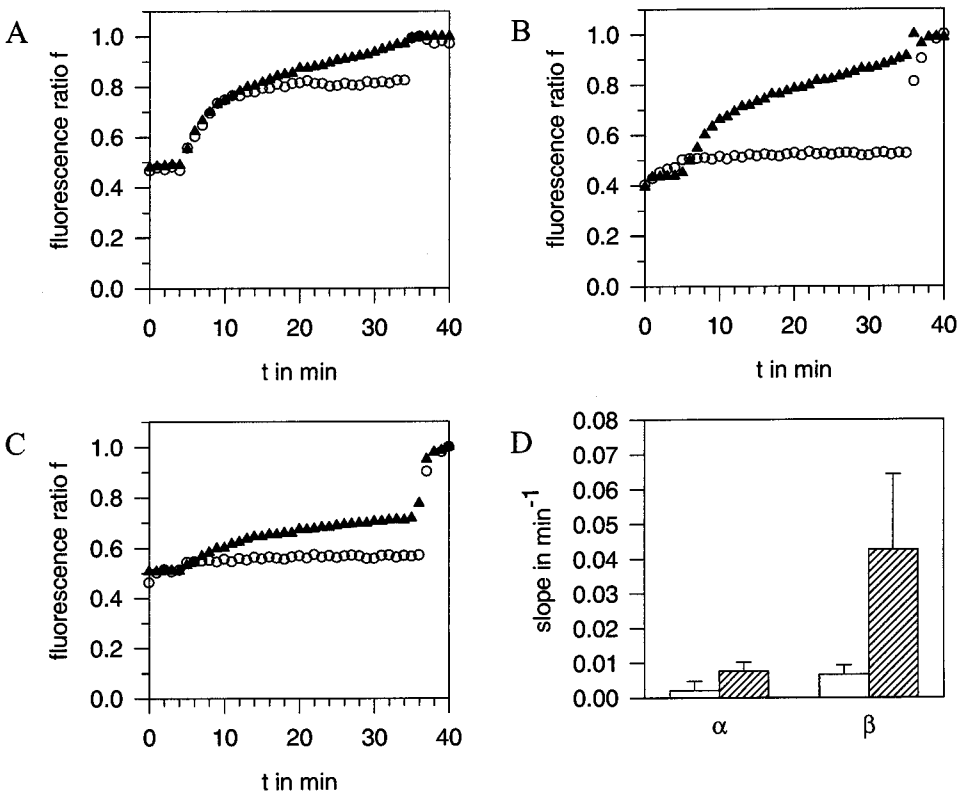

FIGURE 5: Results from the calcium-influx assay for annexin A3 wild-type and the W5A mutant. (A−C) Each panel shows calcium-influx curves for wild-type (white circles) and W5A mutant (black triangles) from one experiment. (D) Analysis of calcium-influx curves for wild-type (white) and W5A mutant (striped): α is the "steady-state" and β the initial slope. Error bars were calculated from the three independent measurements presented in (A−C).

in their attachment to the membrane surface, which in turn alters the permeability of the lipid bilayer.

We tested the electrophysiological activity of annexin A3 wild-type and mutant with di- and monovalent cations and found the conductances for all ions to be in the same range. Exchanging the anion chloride for sulfate revealed the same electrophysiological parameters, which leads to the conclusion that the charge is carried by the cations as already known for other annexins (*42*−*44*). Estimation of ion selectivity based on the reversal potential was not attempted since currents around 0 mV are small and precise determination of the reversal potential proves difficult. The interpretation of electrophysiological results with annexins is not at all simple, therefore preventing straightforward explanations. The current recordings for annexin A3 mutant protein at constant transmembrane potentials clearly show higher membrane permeabilizing activity in comparison with wild-type protein.

A general problem with electrophysiological experiments using annexins is the rare frequency of permeabilizing activity. Rojas and co-workers (*44*) reported a success quota of about 6% at high calcium concentrations (50 mM). A very important observation in this respect is the fact that inactive preparations have a significantly higher seal resistance than active ones. Furthermore, the seal resistance changes to higher values when annexin and calcium are added to a membrane seal. Since at high protein and calcium concentrations annexin molecules form two-dimensional crystals (*13*), we can assume that the high-seal conditions correspond to the formation of a relatively rigid, perhaps semicrystalline, layer of annexin molecules. Recently, we have been able to show that the resistance change represents the voltage-dependent binding of annexins to the membrane (*45*). As this binding is calcium-mediated, the calcium concentration also plays an important role in the adsorption process. When studying different annexins with the preparation procedure described in our paper, the success quota for measurable active annexin seals is 10-fold higher than with the high-calcium protocol of earlier reports (*44*). Thus, it is the ratio of annexin and calcium concentration and the effective membrane area available for annexin binding which are the critical parameters in electrophysiological experiments on annexins.

In conclusion, we show that annexin A3, and especially its mutant W5A, displays membrane permeabilizing activity under appropriate conditions. The activity is due to an annexin-induced cation flow through the membrane, but it is highly sensitive to the ratio of protein, calcium, and membrane surface area. As revealed by the calcium-influx assay, the ability of the mutant to cause calcium influx into PS/PE liposomes is higher than that of the wild-type annexin A3. Furthermore, the inhibitory effect of the W5A mutant on phospholipase A_2 activity is significantly higher than that of the wild-type. The enhanced influx activity of the mutant may therefore be due to better membrane binding inducing higher ion permeability.

The crystal structure of the mutant shows that in the absence of Trp-5 the N-terminal segment is disordered, while our urea-induced unfolding study reveals the importance of the N-terminal tryptophan for the stability of the entire protein. Both the structural and the functional data suggest that the N-terminal region of annexin A3 is indeed involved

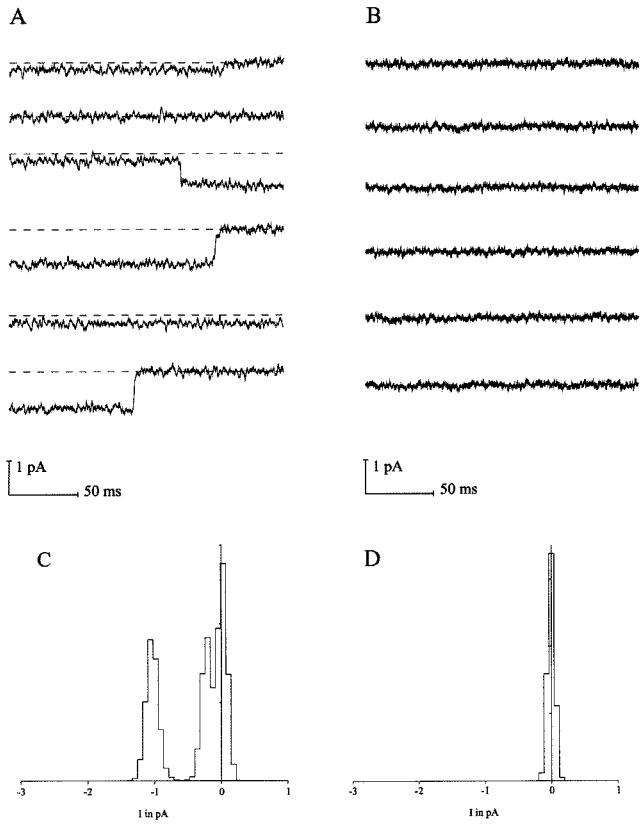

FIGURE 6: Comparison of current recordings from PS/PE (4:1) seals with annexin A3 wild-type and the W5A mutant. The clamped transmembrane potential is −120 mV; the ionic conditions are 100 mM NaCl in the bath and 50 mM $MgCl_2$ in the pipet; the buffer is 10 mM HEPES, pH 7.4. Refiltering was done at 500 Hz. Sections from current recordings with the mutant (A) and the wild-type (B). Typical all-points-amplitude histograms for both proteins (C, mutant; D, wild-type).

in the modulation of membrane permeabilization activity, but it remains to be elucidated what changes take place at the molecular level. It is quite clear that the N-terminal region is a major regulatory element within annexins and it is possible that the various functions of these proteins are modulated via allosteric effects.

ACKNOWLEDGMENT

We thank Lonnie P. Wollmuth, State University of New York at Stony Brook, Stony Brook, NY, as well as Jacques Gallay and Jana Sopkova, LURE, Orsay, France, for helpful discussions. We also thank the groups of Luis Moroder, Max-Planck-Institut für Biochemie, Martinsried, Germany, and George Pavlakis, NCI−FCRDC, Frederick, MD, for access to their luminescence spectrometers. We thank Piotr Bregestovski, Pasteur Institute, Paris, France, for a critical reading of the manuscript. A.H. dedicates this paper to Andrea for her invaluable support.

REFERENCES

1. Moss, S. E. (1992) The Annexins. in *The Annexins* (Moss, S. E., Ed.) 1st ed., pp 1−10, Portland Press, London.
2. Gerke, V., and Moss, S. E. (1997) *Biochim. Biophys. Acta 1357*, 129−154.
3. Crompton, M. R., Moss, S. E., and Crumpton, M. J. (1988) *Cell 55*, 1−3.
4. Barton, G. J., Newman, R. H., Freemont, P. S., and Crumpton, M. J. (1991) *Eur. J. Biochem. 198*, 749−760.
5. Creutz, C. E. (1992) *Science 258*, 924−931.
6. Gerke, V. (1992) Evolutionary conservation and three-dimensional folding of the tyrosine kinase substrate annexin II. in *The Annexins* (Moss, S. E., Ed.) Portland Press, London.
7. Keutzer, J. C., and Hirschhorn, R. R. (1990) *Exp. Cell Res. 188*, 153−159.
8. Pollard, H. B., and Rojas, E. (1988) *Proc. Natl. Acad. Sci. U.S.A. 85*, 2974−2978.
9. Pollard, H. B., Burns, A. L., and Rojas, E. (1990) *J. Membr. Biol. 117*, 101−112.
10. Benz, J., Bergner, A., Hofmann, A., Demange, P., Göttig, P., Liemann, S., Huber, R., and Voges, D. (1996) *J. Mol. Biol. 260*, 638−643.
11. Arispe, N., Rojas, E., Genge, B. R., Wu, L. N. Y., and Wuthier, R. E. (1996) *Biophys. J. 71*, 1764−1775.
12. Pollard, H. B., Guy, H. R., Arispe, N., de la Fuente, M., Lee, G., Rojas, E. M., Pollard, P. R., Srivastava, M., Zhang-Keck, Z. Y., Merezhinskaya, N., Caohuy, H., Burns, A. L., and Rojas, E. (1992) *Biophys. J. 62*, 15−18.
13. Voges, D., Berendes, R., Burger, A., Demange, P., Baumeister, W., and Huber, R. (1994*) J. Mol. Biol. 238*, 199−213.
14. Huber, R., Berendes, R., Burger, A., Schneider, M., Karshikov, A., Lücke, H., Römisch, J., and Paques, E. (1992) *J. Mol. Biol. 223*, 683−704.
15. Berendes, R., Voges, D., Demange, P., Huber, R., and Burger, A. (1993) *Science 262*, 427−430.
16. Karshikov, A., Berendes, R., Burger, A., Cavalié, A., Lux, H. D., and Huber, R. (1992*) Eur. Biophys. J. 20*, 337−344.
17. Lücke, H., Chang, B. T., Mailliard, W. S., Schlaepfer, D. D., and Haigler, H. T. (1995) *Nature 378*, 512−515.
18. Isas, J. M., Cartailler, J. P., Sokolov, Y., Patel, D. R., Langen, R., Lücke, H., Hall, J. E., and Haigler, H. T. (2000) *Biochemistry 39*, 3015−3022.
19. Langen, R., Isas, J. M., Hubbell, W. L., and Haigler, H. T. (1998) *Proc. Natl. Acad. Sci. U.S.A. 95*, 14060−14065.
20. Favier-Perron, B., Lewit-Bentley, A., and Russo-Marie, F. (1996) *Biochemistry 35*, 1740−1744.
21. Kunkel, T. A. (1985) *Proc. Natl. Acad. Sci. U.S.A. 82*, 488−492.
22. Radvanyi, F., Jordan, L., Russo-Marie, F., and Bon, C. (1989) *Anal. Biochem. 177*, 103−109.
23. Dubois, T., Mira, J.-P., Feliers, D., Solito, E., Russo-Marie, F., and Oudinet, J.-P. (1998) *Biochem. J. 330*, 1277−1282.
24. Kerboeuf, D., and Cohen, J. (1990) *J. Cell Biol. 111*, 2527−2535.
25. Portzehl, H., Caldwell, P., and Rüegg, J. (1964) *Biochim. Biophys. Acta 79*, 581−591.
26. Reeves, J. P., and Dowben, R. M. (1968) *J. Cell. Physiol. 73*, 49−60.
27. Grynkiewicz, G., Poenie, M., and Tsien, R. Y. (1985) *J. Biol. Chem. 260*, 3440−3450.
28. Berendes, R., Burger, A., Voges, D., Demange, P., and Huber, R. (1993) *FEBS Lett. 317*, 131−134.
29. Hamill, O. P., Marty, A., Neher, E., Sakmann, B., and Sigworth, F. J. (1981) *Pflügers Arch. 391*, 85−100.
30. Suarez-Isla, B., Wan, K., Lindstrom, J., and Montal, M. (1983) *Biochemistry 22*, 2319−2323.
31. Bazzi, M., and Nelsestuen, G. L. (1991) *Biochemistry 30*, 971−979.
32. Fourme, R., Dhez, P., Benoit, J. P., Kahn, R., Dubuisson, J. M., Besson, P., and Frouin, J. (1992) *Rev. Sci. Instrum. 63*, 982−987.
33. Kabsch, W. (1993) *J. Appl. Crystallogr. 21*, 916−924.
34. CCP4 (1979) *The S.E.R.C. (UK) Collaborative Computing Project No. 4*, Daresbury, U.K.
35. Brünger, A. T., Kuriyan, M., and Karplus, M. (1987) *Science 235*, 458−460.
36. Jones, T. A. (1978) *J. Appl. Crystallogr. 11*, 268−272.
37. Konnert, J. H., and Hendrickson, W. A. (1980) *Acta Crystallogr. A36*, 344−350.
38. Perron, B., Lewit-Bentley, A., Geny, B., and Russo-Marie, F. (1997) *J. Biol. Chem. 272*, 11321−11326.

39. Hofmann, A., Benz, J., Escherich, A., Moroder, L., and Huber, R. (1998) *Fifth European Symposium on Calcium Binding Proteins in Normal and Transformed Cells*, Münster, Germany.
40. Arboledas, D., Olma, N., Lizarbe, M. A., and Turnay, J. (1997) *FEBS Lett. 416*, 217−220.
41. Benz, J., Hofmann, A., Gabler, S., Voges, D., Göttig, P., Bringemeier, I., Liemann, S., Huber, R., and Burger A. (1999) in preparation.
42. Burger, A., Voges, D., Demange, P., Perez, C. R., Huber, R., and Berendes, R. (1994) *J. Mol. Biol. 237*, 479−499.
43. Liemann, S., Benz, J., Burger, A., Voges, D., Hofmann, A., Huber, R., and Göttig, P. (1996) *J. Mol. Biol. 258*, 555−561.
44. Rojas, E., Pollard, H. B., Haigler, H. T., Parra, C., and Burns, A. L. (1990) *J. Biol. Chem. 265*, 21207−21215.
45. Hofmann, A., Benz, J., Liemann, S., and Huber, R. (1997) *Biochim. Biophys. Acta 1330*, 254−264.
46. Brünger, A. T. (1992) *Nature 355*, 472−474.
47. Kraulis, P. J. (1991) *J. Appl. Crystallogr. 24*, 946−950.
48. Morgan, R. O., Jenkins, N. A., Gilbert, D. J., Copeland, N. G., Balsara, B. R., Testa, J. R., and Fernandez, M. P. (1999) Novel human and mouse annexin A10 are linked to the genome duplications during early chordate evolution. *Genomics 60*, 40−49.

BI992359+